$p-CoO_xIn-SnO_2$ nanostructures : new highly selective materials for H_2S detection

p-CoO_x/*n*-SnO_2 nanostructures: new highly selective materials for H_2S detection

M.N. Rumyantseva[a,*], S.A. Vladimirova[a], N.A. Vorobyeva[a], I. Giebelhaus[b], S. Mathur[b], A.S. Chizhov[a], N.O. Khmelevsky[c], A.Yu. Aksenenko[c], V.F. Kozlovsky[a], O.M. Karakulina[d], J. Hadermann[d], A.M. Abakumov[d,e], A.M. Gaskov[a]

[a]*Chemistry Department, Moscow State University, Moscow 119991 Russia*

[b]*Institute of Inorganic Chemistry, University of Cologne, D-50939 Cologne, Germany*

[c]*LISM, Moscow State Technological University Stankin, 127055 Moscow, Russia*

[d]*EMAT, University of Antwerp, B-2020 Antwerp, Belgium*

[e]*Skolkovo Institute of Science and Technology, 143026 Moscow, Russia*

Abstract

Nanostructures *p*-CoO_x/*n*-SnO_2 based on tin oxide nanowires have been prepared by two step CVD technique and characterized in detail by XRD, XRF, XPS, HAADF-STEM imaging and EDX-STEM mapping. Depending on the temperature of decomposition of cobalt complex during the second step of CVD synthesis of nanostructures cobalt oxide forms a coating and/or isolated nanoparticles on SnO_2 nanowire surface. It was found that cobalt presents in +2 and +3 oxidation states. The measurements of gas sensor properties have been carried out during exposure to CO (14 ppm), NH_3 (21 ppm), and H_2S (2 ppm) in dry air. The opposite trends were observed in the effect of cobalt oxide on the SnO_2 gas sensitivity when detecting CO or NH_3 in comparison to H_2S. The decrease of sensor signal toward CO and NH_3 was attributed to high catalytic activity of Co_3O_4 in oxidation of these gases. Contrary, the significant increase of sensor signal in the presence of H_2S was attributed to the formation of metallic cobalt sulfide and removal of the barrier between *p*-CoO_x and *n*-SnO_2. This effect provides an excellent selectivity of *p*-CoO_x/*n*-SnO_2 nanostructures in H_2S detection.

Keywords: nanostructured materials; tin dioxide nanowires; cobalt oxide; *p* – *n* heterojunction; H_2S; semiconductor gas sensor

[*] Corresponding author. Tel: +7 495 939 54 71, Fax: +7 495 939 09 98. E-mail address: roum@inorg.chem.msu.ru

1. Introduction

Resistive gas sensors based on wide gap semiconductor metal oxides are extensively used in different applications due to their high sensitivity combined with simple and cost effective device configurations. The main disadvantage of this technology is poor selectivity caused by non-specific interaction with gasses of different chemical nature. One of the ways to enhance the selectivity of wide gap semiconducting oxides is the surface modification and the development of complex nonhomogeneous systems (nanocomposites or nanostructures) [1,2]. The improvements in sensing performance of these nanostructures have been attributed to many factors [3], which include (i) electronic effects such as: band bending due to Fermi level equilibration, charge carrier separation, depletion layer change and increased interfacial potential barrier energy; (ii) chemical effects, namely a decrease in activation energy, targeted catalytic activity and synergistic surface reactions; and (iii) geometrical effects such as grain refinement, surface area enhancement, and increased gas accessibility.

A very common interface used to alter gas sensing properties is a p – n junction. N-type (SnO_2, ZnO, TiO_2, In_2O_3, WO_3) and p-type (Cr_2O_3, Co_3O_4, NiO, CuO, PdO, Ag_2O, CdO) semiconductor oxides can be combined in different ways to utilize the effects of the junction and improve sensing performance [3]. Nanocomposites based on tin dioxide SnO_2 and cobalt oxides CoO or Co_3O_4 are of particular interest since they combine the feasibility of both electronic and chemical sensitization. SnO_2 as *n*-type and CoO and Co_3O_4 as *p*-type semiconductors form a *p* – *n* junction with a depletion region at the interface, whose characteristics depend on the respective Fermi level positions. Besides, it is known that Co_3O_4 is catalytically active in low temperature oxidation of CO and NH_3 [4-6], and it is a promising material for water oxidation catalysts [7] and adsorbents for low temperature gas desulfurization [8,9]. The gas sensor properties of nanocrystalline materials based on cobalt-doped tin dioxide were previously investigated toward CO [10,11], H_2 [10-14], ozone [14] and acetone vapour [15]. It was revealed that this doping can be accompanied by either improvement of sensor parameters at low cobalt concentration levels, or by degradation of sensor characteristics, when the cobalt concentration exceeds its solubility limit in SnO_2 [14].

In this paper we investigated the gas sensor properties of nanostructures CoO_x/SnO_2 based on tin oxide nanowires toward CO, NH_3, and H_2S. Gas sensor performance of CoO_x/SnO_2 nanowires towards H_2S was studied for the first time and analyzed in terms of the role of the *p* – *n* heterojunction in sensor signal formation.

2. Experimental

2.1 Materials synthesis

Nanowire-based nanocomposites were produced following a two-step chemical vapor deposition (CVD) of corresponding metal organic precursors. In the initial step, single-crystalline tin oxide nanowires were deposited by a metal-seeded vapor–liquid–solid growth mechanism using $Sn(OBut)_4$ as a precursor ($T_{substrate}$ = 750 ^oC, $T_{precursor}$ = 25 ^oC, t = 30 min) on Al_2O_3 substrates covered with gold nanoparticles [16]. In a subsequent step, cobalt nanoparticles were deposited on pre-grown SnO_2 nanowires by the CVD of $CoC_{22}H_{26}N_4O_2F_6$ (Fig.1), in accordance with the procedure described earlier ($T_{substrate}$ = 500 or 600 ^oC, $T_{precursor}$ = 150^oC, t = 20 min) [17]. The resulting SnO_2 nanowires decorated with cobalt particles were annealed in air at 450 ^oC for 24 h.

In accordance with the preassigned atomic cobalt content (*X*) and the temperature of cobalt particles deposition the nanostructures are named as CoXSn-nw500 and CoXSn-nw600 (Table 1).

2.2. Methods

The specimens for transmission electron microscopy (TEM) were prepared by dispersing powders in ethanol. Prior to this, the nanowires were scratched off the substrates, and crushed in a mortar. A few drops of the resulting dispersion solution were deposited on a copper grid covered with a holey-carbon film. High angle annular dark field scanning TEM (HAADF-STEM) images and energy dispersive X-ray spectroscopy (EDX-STEM) maps were acquired at a Titan G^3-cubed transmission electron microscope operating at 300 kV. The instrument was equipped with Super-X detectors.

The ratio of concentrations [Co]/([Co]+[Sn]), at.% was determined by X-ray fluorescent analysis (XRF) on a M1 Mistral spectrometer (Bruker) with the beam energy of 50 keV.

Phase composition was determined by X-ray powder diffraction (Rigaku diffractometer, monochromatized Cu $K_{\alpha 1}$ radiation, λ=1.5406 Å). The crystallite size (d_{XRD}) was calculated from the broadening of the most intensive XRD peaks of the SnO_2 (110, d = 3.347 Å) and Co_3O_4 (311, d = 2.437 Å) phases using the Scherrer equation.

X-ray photoelectron spectroscopy (XPS) measurements were performed using a K-Alpha (Thermo Scientific) spectrometer equipped with a monochromatic Al K_α X-ray source (E = 1486.7 eV). Charge neutralization was applied, providing the C1s peak position of 285.0 eV. XP-spectra were fitted by Gaussian – Lorentzian convolution functions with simultaneous optimization of the background parameters.

For the gas sensing experiments, the nanowires were scratched off the Al_2O_3 substrate, mixed with a vehicle (α-terpineol in ethanol) and deposited by drop coating technique over functional alumina substrates (~ 120 μm thick), having Pt contacts on the front side and a Pt-meander on the back-side, which acts both as a heating element and a temperature probe. The thick films were dried at 30 ^oC for 24h and sintered at 450 ^oC for 10h in air. All sensor measurements have been carried out by flow-through technique under a controlled constant flux of 100 ml/min. The atmosphere composition was pre-assigned by means of electronic mass-flow controllers (Bronkhorst). They mixed flows coming from certified bottles, which contained a given amount of the target gas diluted in synthetic air with the background flow. The background atmosphere was obtained from a pure air generator. DC volt-amperometric measurements (U = 3 V) have been carried out to monitor the electrical conductance of the sample during exposure to CO (14 ppm), NH_3 (21 ppm), and H_2S (2 ppm) in dry air. The response S of the sensor was calculated as $S = (G_{gas} - G_{air})/G_{air}$, where G_{gas} is the conductance of the sample in the presence of reducing gas, G_{air} is the conductance in pure air.

3. Results and discussion

3.1. Samples characterization

HAADF-STEM images and EDX-STEM maps of the Co5Sn-nw500 and Co10Sn-nw600 are shown in Fig. 2 and Fig. 3. The Co5Sn-nw500 sample consists of crystalline SnO_2 nanowires with a diameter ranging from 10 to 50 nm. The surface of SnO_2 nanowires is coated with a ~1-2 nm continuous layer of cobalt oxide. The cobalt oxide nanoparticles are practically absent in this sample. In the Co10Sn-nw600 sample, both cobalt oxide particles and an irregular cobalt oxide coating (also ~1-2 nm thickness) are present at the surface of the SnO_2 nanowires. Such a difference in cobalt distribution on the surface of SnO_2 nanowires may be caused by the temperature of decomposition of cobalt complex during the second step of CVD synthesis of nanostructures.

Fig. 4 shows the X-ray powder diffraction patterns of the CoXSn-nw nanostructures. Co5Sn-nw500 sample with lower cobalt content contain only one crystalline phase, i.e. SnO_2 (ICDD 41-1445, cassiterite). In the XRD pattern of Co10Sn-nw600 nanostructures, diffraction peaks corresponding to the Co_3O_4 phase (ICDD 42-1467) can be found. The phase composition and average crystallite size (d_{XRD}) of SnO_2 and Co_3O_4 phases determined from XRD spectra are presented in Table 1. The lattice parameters of SnO_2 in the Co5Sn-nw500 and Co10Sn-nw600 nanostructures have been determined from the X-ray diffraction patterns (Table 1). No change of

SnO_2 lattice parameters is observed. This is consistent with the results of EDX-STEM mapping, which showed that cobalt is located on the surface of SnO_2 nanowires.

The electronic state of the elements in Co10Sn-nw600 was examined by XPS method (Fig. 5). The positions of the peaks Sn $3d_{5/2}$ (486.6 eV) and Sn $3d_{3/2}$ (495.0 eV) correspond to Sn (IV) [18]. Oxygen in the XP-spectra of the samples exhibits an asymmetric O 1s signal. The main peak (530.4 eV) refers to the SnO_2 lattice oxygen anions [18]. The second one (531.7 eV) is due to the presence of various forms of oxygen adsorbed on the SnO_2 surface.

Since Co(II) and Co(III) have very similar Co-2p binding energies, the unambiguous determination of cobalt oxidation state is hampered. However, there are two clear features in the 2p core level XP-spectra that allow us to distinguish between Co(II) and Co(III) [19]. First, the Co(II) 2p core level exhibits a strong shake-up satellite peak towards higher binding energy in contrast to Co(III) 2p, which exhibits only a weak satellite. Second, the separation of the Co $2p_{1/2}$–$2p_{3/2}$ spin-orbit components is about 16.0 eV for Co(II) and 15.0 eV for Co(III). The XP-spectra of the Co10Sn-nw600 nanostructures in the Co 2p binding energy region are shown in Fig. 6. In this case, experimental curves can be fitted 4 doublets corresponding to Co(III) and Co(II) main peaks and Co(II) shake-up satellites. Table 2 presents the Co $2p_{3/2}$ XPS spectral assignments and spin orbit splittings for Co10Sn-nw600 sample. By comparison of the estimated Co $2p_{3/2}$ binding energies with reference data [20,21] one can conclude that cobalt is present in oxidation state +2 and +3, wherein the environment of Co(II) meets both the structure of CoO, and Co_3O_4.

3.2. Electrical and gas sensor properties

Fig. 6 illustrates the electrical response of SnO_2 nanowires and CoXSn-nw nanostructures to the periodical change of gas phase composition from dry air to gas mixtures containing CO (14 ppm), NH_3 (21 ppm), or H_2S (2 ppm) in dry air in the temperature range of 150 – 450 °C. It is necessary to note that the introduction of cobalt results in a significant growth of nanostructure resistance as compared with SnO_2 nanowires. At 350 ^oC the resistance in pure air is $1*10^7$, $3*10^8$ and $1*10^9$ Ohm for SnO_2, Co5Sn-nw500, and Co10Sn-nw600 film, respectively. As it was demonstrated, cobalt is located on the surface of SnO_2 nanowires, so the possibility of *p*-CoO or *p*-Co_3O_4 formation must be considered, since it leads to the formation of an electrical barrier at the contacts between *n*-SnO_2 (work function 4.7 eV, band gap 3.6 eV) and *p*-Co_3O_4 (work function 6.1 eV, band gap 1.6 eV) or *p*-CoO (work function 4.5 eV, band gap 2.4 eV) [22,23]. In this case the *p*-type semiconductor dopes *n*-SnO_2 with holes compensating available donors near the surface. As a result, the surface potential and the thickness *W* of the space charge region (SCR) increase, and consequently the resistivity rises. Concerning the nanowires, the ratio

between their diameter *D* and the SCR width *W* determines the effective conduction channel. It is reduced by the extension of the depleted region, that leads to a higher resistance. For thick films prepared from nanowires the electron transport is modulated by potential barriers between the nanowires [24,25]:

$$G_{air} \propto \frac{e\mu n_0 (D-W)^2}{l} \exp\left(-\frac{eV_s}{kT}\right) \quad (1)$$

where μ is the carrier mobility, l is the distance between electrodes, V_s is band bending induced by oxygen chemisorption.

According to the resistance response toward reducing gases CO (14 ppm), NH_3 (21 ppm), and H_2S (2 ppm), all investigated samples behave as *n*-type semiconductors. A decrease in the electrical resistance in the presence of reducing gas could be explained by the following redox reactions:

$$\beta \cdot \mathrm{CO}_{(gas)} + \mathrm{O}^{-\alpha}_{\beta(ads)} \rightarrow \beta \cdot \mathrm{CO}_{2(gas)} + \alpha \cdot e^{-}, \quad (2a)$$

$$2\beta \cdot NH_{3(gas)} + 3O^{-\alpha}_{\beta(ads)} \rightarrow \beta \cdot N_{2(gas)} + 3\beta \cdot H_2O_{(gas)} + 3\alpha \cdot e^{-} \quad (2b)$$

$$\beta \cdot H_2S_{(gas)} + 3O^{-\alpha}_{\beta(ads)} \rightarrow \beta \cdot SO_{2(gas)} + \beta \cdot H_2O_{(gas)} + 3\alpha \cdot e^{-}, \quad (2c)$$

where $CO_{(gas)}, NH_{3(gas)}, H_2S_{(gas)}$ represent the reducing gas molecule in the gas phase, $\mathrm{O}^{-\alpha}_{\beta(ads)}$ is an atomic or molecular form of chemisorbed oxygen, $CO_{2(gas)}, SO_{2(gas)}, N_{2(gas)}, H_2O_{(gas)}$ are the molecules of reaction products, *e* is an electron injected into the conduction band of the semiconductor.

Fig. 7 illustrates the temperature dependences of sensor signal *S* of SnO_2 nanowires and CoXSn-nw nanostructures to CO (14 ppm), NH_3 (21 ppm), and H_2S (2 ppm). The opposite trend is noted in the effect of cobalt on the SnO_2 gas sensitivity when detecting CO or NH_3 in comparison to H_2S. Fig. 8 compares the maximum values of sensor signal to different reducing gases for bare SnO_2 and CoXSn-nw nanostructure. One can observe the reduced sensor signal to CO or NH_3 for cobalt containing samples. Such behavior should be attributed to high catalytic activity of Co_3O_4 in oxidation of CO and NH_3. In a detailed review [4] the high activity of Co_3O_4 in low temperature CO oxidation is explained by relatively low barriers for surface reaction and by the fact that O_2 adsorption on Co_3O_4 is never inhibited by CO as observed for all noble metals. Busca et al. confirmed that the surface of Co_3O_4 is highly oxidized [5]. Excess oxygen in Co_3O_{4+x} could be located in a relatively thin surface layer coupled with Co^{3+} ions. This surface is very reactive, even with respect to stable molecules such as ammonia, which rapidly decomposes at room temperature. This agrees with the very high catalytic activity of Co_3O_4 towards ammonia combustion, and is probably related to the instability of Co^{3+} ions that tend to be reduced to Co^{2+}.

Reducing of Co_3O_4 to CoO leads to catalyst deactivation [6]. Considering the catalytic activity of Co_3O_4, it can be concluded that during CO and NH_3 detection these molecules are directly oxidized at the surface of the Co_3O_4 particles. This leads to the decrease in the quantity of CO and NH_3 molecules which can react with the oxygen chemisorbed on SnO_2 surface, and consequently to the decrease in sensor signal of CoXSn-nw nanostructures comparing with SnO_2 nanowires.

Maximum sensor signal *S* to 2 ppm H_2S rises *S* = 40 for SnO_2 nanowires to *S* = 1000 for Co10Sn-nw600 nanostructure. This indicates that an additional sensing mechanism is realized, in which cobalt oxide is involved. A recent study of Co_3O_4-based materials showed that they act as effective sorbents for low temperature gas desulfurisation including conditions of excess of ammonia and water vapor [8,9,26]. Furthermore, their activity is superior even at room temperature. Baird et al. [9] demonstrated that Co_3O_4 reacts stoichiometrically with H_2S at 30°C but the reaction depth is only 3.7 monolayers (about 0.4 nm). Therefore, the sulfur uptake is very sensitive to the surface area of cobalt oxide. According to XPS studies of the sulfurized oxides, H_2S reduces the surface of spinel Co_3O_4 to rock salt CoO prior to the formation of cobalt sulfides [9]. At the same time sulfur forms, which oxidizes to SO_2 or surface sulfate, in the presence of oxygen excess. Taking into account this interaction between Co_3O_4 and gaseous H_2S one can conclude that the mechanism of sensor signal formation in CoO_x/SnO_2 nanocomposites is similar to that established for CuO/SnO_2 materials obtained in different forms: ceramics and thick films [27-30], thin films [31-33], planar thin films heterostructures [34], and 1D nanostructures [35-39]. So the high sensor response to H_2S may be caused by two complementary contributions: (i) chemical interaction between cobalt oxide and H_2S:

$$Co_3O_4 + H_2S_{(gas)} + O_{2(gas)} = 3CoO + SO_{2(gas)} + H_2O_{(gas)} \quad (3)$$

$$CoO + H_2S_{(gas)} = CoS + H_2O_{(gas)} \quad (4)$$

and (ii) the properties of *p*-CoO_x/*n*-SnO_2 heterojunction.

In equation (4) “CoS” denotes a cobalt (II) sulfide. A large number of cobalt sulfides have been reported but not all of them have been fully characterized [40]. Cobalt gives rise to CoS_2 with the pyrites structure, Co_3S_4 with the spinel structure, and $Co_{1-x}S$, which has the NiAs structure and is cobalt deficient. All are metallic as Co_9S_8. The standard enthalpies of formation of different bulk cobalt sulfides (normalized per one cobalt atom) determined by high temperature direct reaction calorimetry have been reported by Cemič and Kleppa [41]: $\Delta H^0_f(Co_{0.934}S)$ = – 106.45 ± 1.63 kJ/mol, $\Delta H^0_f(Co_9S_8)$ = – 98.41 ± 1.87 kJ/mol, $\Delta H^0_f(Co_3S_4)$ = – 115.82 ± 2.42 kJ/mol, $\Delta H^0_f(CoS_2)$ = – 150.94 ± 4.85 kJ/mol. From a thermodynamic point of

view the formation of CoS_2 is the most favorable. However, for nanocrystalline systems the surface energy contributes considerably and uncontrollably which can significantly change the situation.

To verify the proposed sensing mechanism and to confirm the formation of a certain cobalt sulfide under sensor measurement conditions, an additional experiment was performed. For this purpose powder based nanocomposite Co10Sn750 was synthesized. Tin dioxide powder was prepared by conventional hydrolysis of $SnCl_4$ [42] with subsequent annealing at 750 ^oC for 24h. After that, the cobalt was introduced with concentration corresponding to X = [Co]/([Co]+[Sn]) = 10 at.% by wetness impregnation procedure using $Co(NO_3)_2$ solution. Then, the powder was calcined in air at 450 ^oC for 24 h. Thus obtained Co10Sn750 nanocomposite was annealed in H_2S containing atmosphere (2 ppm in air) at 250 ^oC for 1 h, cooled to room temperature in the same gas mixture, and immediately subjected to XRD examination. Fig. 9 compares the X-ray diffraction patterns of the Co10Sn750 sample before and after interaction with H_2S. One can conclude that as a result of reaction with H_2S the oxide phase Co_3O_4 disappears and a cobalt sulfide phase is formed. Phase analysis using the ICDD database revealed that the most probable is the formation of a cobalt deficient sulfide with hexagonal structure. The recovery of the electrical characteristics of the sensor material in pure air (in the absence of H_2S) observed for all the samples serves as a proof of reversibility of this interaction.

In any case, the chemical transformation from *p*-CoO_x to metallic cobalt sulfide results in the removal of the p – n junction (Fig. 10) and in a growth in SnO_2 conductivity. It should be noted that such removal of the barrier is only possible in the presence of sulfur containing reducing gases as H_2S and, possibly, mercaptans. Indeed, the interaction with other reducing gases (CO, H_2, NH_3) will result only in the reduction of Co_3O_4 to CoO [4-6]. As the latter is also a *p*-type semiconductor, such transformation will not lead to the effective removal of the barrier. So this mechanism of sensor signal formation will not be realized. Thus nanocomposites based on tin and cobalt oxides are promising gas sensor materials for selective detection of hydrogen sulfide, even in the presence of other reducing gases. This point requires the experimental verification, which will be done in future work.

Conclusions

Nanostructures *p*-CoO_x/*n*-SnO_2 based on tin oxide nanowires with a diameter of 10 – 50 nm have been prepared by two step CVD technique, and characterized in detail using XRD, XRF, XPS, HAADF-STEM imaging and EDX-STEM. It was found that cobalt is localized on the surface of SnO_2 nanowires and present in +2 and +3 oxidation states.

During CO and NH_3 detection, these gas molecules are directly oxidized at the surface of the Co_3O_4 particles while the SnO_2 matrix is not involved in the oxidation process. This reduces the sensor signal of *p*-CoO_x/*n*-SnO_2 nanostructures compared to bare tin dioxide nanowires. In the case of H_2S detection the mechanism of sensor signal formation in *p*-CoO_x/*n*-SnO_2 nanostructures is similar to that established for CuO/SnO_2 materials. High sensor response to H_2S may be caused by two complementary contributions: (i) chemical interaction between cobalt oxide and H_2S and (ii) the properties of the *p*-CoO_x/*n*-SnO_2 heterojunction. The chemical transformation from *p*-CoO_x to metallic cobalt sulfide results in the removal of the *p* – *n* junction and in an increase in the SnO_2 conductivity. This effect provides an excellent selectivity of nanocomposites based on tin and cobalt oxides in H_2S detection.

Acknowledgements

This work was supported by ERA-Net.Plus grant no. 096 FONSENS.

References

[1] M.N. Rumyantseva, A.M. Gaskov, Chemical modification of nanocrystalline metal oxides: effect of the real structure and surface chemistry on the sensor properties, Russ. Chem. Bull. 57 (2008) 1086–1105.

[2] R.B. Vasiliev, M.N. Rumyantseva, L.I. Ryabova, A.M. Gaskov, Inorganic structures as materials for gas sensors, Russ. Chem. Rev.73 (2004) 939–956.

[3] D.R. Miller, Sh.A. Akbar, P.A. Morris, Nanoscale metal oxide – based heterojunctions for gas sensing: A review, Sens. Actuators B 204 (2014) 250–272.

[4] S. Royer, D. Duprez, Catalytic oxidation of carbon monoxide over transition metal oxides, ChemCatChem 3 (2011) 24–65.

[5] G. Busca, R. Guidetti, V. Lorenzelli, Fourier-transform Infrared Study of the Surface Properties of Cobalt Oxides, J. Chem. Soc. Faraday Trans.86 (1990) 989–994.

[6] K. Schmidt-Szałowski, K. Krawczyk, J. Petryk, The properties of cobalt oxide catalyst for ammonia oxidation, Appl. Catal. A 175 (1998) 147–157.

[7] X. Deng, H. Tüysüz, Cobalt-Oxide-Based Materials as Water Oxidation Catalyst: Recent Progress and Challenges, ACS Catal. 4 (2014) 3701–3714.

[8] L.R. Pahalagedara, A.S. Poyraz, W. Song, Ch.-H. Kuo, M.N. Pahalagedara, Yo.-T. Meng, S.L. Suib, Low Temperature Desulfurization of H_2S: High Sorption Capacities by Mesoporous Cobalt Oxide via Increased H_2S Diffusion, Chem. Mater. 26 (2014) 6613–6621.

[9] T. Baird, K.C. Campbell, P.J. Holliman; R.W. Hoyle, M. Huxam, D. Stirling, B.P. Williams, M. Morris, Cobalt–zinc oxide absorbents for low temperature gas desulfurization, J. Mater. Chem. 9 (1999) 599–605.

[10] U.-S. Choi, G. Sakai, K. Shimanoe, N. Yamazoe, Sensing properties of SnO_2–Co_3O_4 composites to CO and H_2, Sens. Actuators B. 98 (2004) 166–173.

[11] S. Abe, U.-S. Choi, K. Shimanoe, N.Yamazoe, Influences of ball-milling time on gas-sensing properties of Co_3O_4–SnO_2 composites, Sens. Actuators B. 107 (2005) 516–522.

[12] L. Liu, Ch. Guo, Sh. Li, L. Wang, Q. Dong, W. Li, Improved H_2 sensing properties of Co-doped SnO_2 nanofibers, Sens. Actuators B. 150 (2010) 806–810.

[13] L.P. Oleksenko, N.P. Maksymovych, A.I. Buvailo, I.P. Matushko, N. Dollahon, Adsorption-semiconductor hydrogen sensors based on nanosized tin dioxide with cobalt oxide additives, Sens. Actuators B. 174 (2012) 39–44.

[14] G. Korotcenkov, I. Boris, V. Brinzari, S.H. Han, B.K. Cho, Adsorption-semiconductor hydrogen sensors based on nanosized tin dioxide with cobalt oxide additives, Sens. Actuators B. 182 (2013) 112–124.

[15] S.B. Patil, P.P. Patil, M.A. More, Adsorption-semiconductor hydrogen sensors based on nanosized tin dioxide with cobalt oxide additives, Sens. Actuators B. 125 (2007) 126–130.

[16] R. Müller, F. Hernandez-Ramirez, H. Shen, H. Du, W. Mader, S. Mathur, Influence of Precursor Chemistry on Morphology and Composition of CVD-Grown SnO_2 Nanowires, Chem. Mater. 24 (2012) 4028–4035.

[17] I. Giebelhaus, Übergangsmetall-Heteroarylalkenolate der Formel $M[(Ar)CHC(R)O]_2$ (M(II) = Co, Ni, Cu, Sn): Neuartige Vorstufen in der Materialsynthese, Ph.D. Thesis, University of Cologne, 2013.

[18] C.D. Wagner, W.M. Riggs, L.E. Davis, G.F. Moulder, Handbook of X-ray Photoelectron Spectroscopy, Perkin Elmer Co, 1979.

[19] M. Batzill, T. James, M. Burst, U. Diebold, Pure and cobalt-doped SnO_2(101) films grown by molecular beam epitaxy on Al_2O_3, Thin Solid Films 484 (2005) 132–139.

[20] T.J. Chuang, C.R. Brundle, V. Rice, Interpretation of the X-Ray photoemission spectra of cobalt oxides and cobalt oxide surfaces, Surf. Sci. 59 (1976) 413–429.

[21] M.C. Biesinger, B.P. Payne, A.P. Grosvenor, L.W.M. Lau, A.R. Gerson, R.St.C. Smart, Resolving surface chemical states in XPS analysis of first row transition metals, oxides and hydroxides: Cr, Mn, Fe, Co and Ni, Appl. Surf. Sci. 257 (2011) 2717–2730.

[22] T. Minami, T. Miyata, T.Yamamoto, Work function of transparent conducting multicomponent oxide thin films prepared by magnetron sputtering, Surf. Coat. Technol. 108 (1998) 583–587.

[23] M.T. Greiner, M.G. Helander, W.-M. Tang, Zh.-B. Wang, J. Qiu, Zh.-H. Lu, Universal energy-level alignment of molecules on metal oxides, Nature Mater. 11 (2011) 75–81.

[24] V.V. Sysoev, B.K. Button, K. Wepsiec, S. Dmitriev, A. Kolmakov, Toward the Nanoscopic "Electronic Nose": Hydrogen vs Carbon Monoxide Discrimination with an Array of Individual Metal Oxide Nano- and Mesowire Sensors, Nano Lett. 6 (2006) 1584–1588.

[25] V.V. Sysoev, T. Schneider, J. Goschnick, I. Kiselev, W. Habicht, H. Hahn, E. Strelcov and A. Kolmakov, Percolating SnO2 nanowire network as a stable gas sensor: Direct comparison of long-term performance *versus* SnO2nanoparticle films, Sens. Actuators B 139 (2009) 699–703.

[26] S.W. Chun, J.Ye. Jang, D.W. Park, H.Ch.Woo, J.S.Chung, Selective oxidation of H_2S in the presence of ammonia and water using Co_3O_4/SiO_2 catalyst, Kor. J. Chem. Eng. 14 (1997) 216–218.

[27] J. Tamaki, T. Maekawa, N. Miura, N. Yamazoe, CuO - SnO_2 element of highly sensitive and selective detection of H_2S, Sens. Actuators B 9 (1992) 197–203.

[28] M. Boulova, A. Galerie, A. Gaskov, G.Lucazeau, Reactivity of SnO_2-CuO nanocrystalline materials with H_2S: a coupled electrical and Raman spectroscopic study, Sens. Actuators B 71 (2000) 134–139.

[29] L.A. Patil, D.R. Patil, Heterocontact type CuO-modified SnO_2 sensor for the detection of a ppm level H_2S gas at room temperature, Sens. Actuators B 120 (2006) 316–323.

[30] H. Liu, S.P. Gong, Y.X.Hu, J.Q. Liu, D.X. Zhou, Properties and mechanism study of SnO_2 nanocrystals for H_2S thick-film sensors, Sens. Actuators B 140 (2009) 190–195.

[31] M.N. Rumyantseva, M. Labeau, G. Delabouglise, L.I. Ryabova, I.B. Kutsenok, A.M.Gaskov, Copper and nickel doping effect on interaction of SnO_2 films with H_2S, J. Mater. Chem. 7 (1997) 1785–1790.

[32] R.S. Nirajan, K.R. Patil, S.R. Sainkar, I.S. Mulla, High H_2S-sensitive copper-doped tin oxide thin film, Mater. Chem. Phys. 80 (2003) 250–256.

[33] V.R. Katti, A.K. Debnath, K.P. Muthe, M. Kaur, A.K. Dua, S.C. Gadkari, S.K. Gupta, V.C. Sahni, Mechanism of drifts in H_2S sensing properties of SnO_2:CuO composite thin film sensors prepared by thermal evaporation, Sens. Actuators B 96 (2003) 245–252.

[34] R.B. Vasiliev, M.N. Rumyantseva, N.V. Yakovlev, A.M.Gaskov, CuO/SnO_2 thin film heterostructures as chemical sensors to H_2S, Sens. Actuators B 50 (1998) 187–194.

[35] S.S. Kim, H.G. Na, S.-W. Choi, D.S. Kwak, H.W. Kim, Novel growth of CuO-functionalized, branched SnO_2 nanowire and their application to H_2S sensors, J. Phys. D. Appl. Phys. 45 (2012) 205301-1–205301-8.

[36] X. Kong, Ya. Li, High sensitivity of CuO modified SnO_2 nanoribbons to H_2S at room temperature, Sens. Actuators B 105 (2005) 449–453.

[37] V. Kumar, S. Sen, K.P. Muthe, N.K. Gaur, S.K. Gupta, J.V. Yakhmi, Copper doped SnO_2 nanowires as highly sensitive H_2S gas sensor Sens. Actuators B 138 (2009) 587–590.

[38] I.S. Hwang, J.K. Choi, S.-J. Kim, K.Y. Dong, J.H. Kwon, B.K. Ju, J.H.Lee, Enhanced H_2S sensing characteristics of SnO_2 nanowires functionalized with CuO, Sens. Actuators B 142 (2009) 105–110.

[39] S. Mathur, I. Giebelhaus, T. Fischer, J.R. Morante, J. Arbiol, A. Gaskov, M. Rumyantseva, E. Varechkina, V. Ivanov, One-dimensional CuO-SnO_2 p-n heterojunctions for enhanced detection of H_2S, J. Mater. Chem. A 1 (2013) 11261–11268.

[40] F. Shao, M.W.G. Hoffmann, J.D. Prades, R. Zamani, J. Arbiol, J.R. Morante, E.Varechkina, M. Rumyantseva, A. Gaskov, I. Giebelhaus, T. Fischer, S. Mathur, F. Hernández-Ramírez, Heterostructured p-CuO (nanoparticle)/n-SnO_2 (nanowire) devices for selective H_2S detection, Sens. Actuators B 181 (2013) 130–135.

[41] N.N. Greenwood and A. Earnshaw, Cobalt, Rhodium and Iridium. In Chemistry of the Elements, Elsevier Science Ltd.: Kidlington, 1997.

[42] L. Cemič, O.J. Kleppa, High Temperature Calorimetry of Sulfide Systems. III. Standard Enthalpies of Formation of Phases in the Systems Fe – Cu – S and Co – S, Phys. Chem. Minerals 16 (1988) 172–179.

[43] M.N. Rumyantseva, A.M. Gaskov, N. Rosman, T. Pagnier, J.R. Morante, Raman surface vibration modes in nanocrystalline SnO_2 prepared by wet chemical methods: correlations with the gas sensors performances, Chem. Mater. 17 (2005) 893–901.

Table 1. Samples designation, composition and microstructure parameters

Sample	[Co]/([Co]+[Sn]), at.%		Phase composition	Crystallite size d_{XRD}, nm
	Preassigned	Determined (XRF)		
Sn-nw	-	-	SnO_2	25 ± 2
Co5Sn-nw500	5	3.4 ± 0.3	SnO_2	25 ± 2
Co10Sn-nw600	10	8.6 ± 0.4	SnO_2	25 ± 2
			Co_3O_4	10 ± 2

Table 2. Co $2p_{3/2}$ XPS spectral assignments

Spectral assignment	Co $2p_{3/2}$ binding energy, eV		
	Ref. 20	Ref. 21	Co10Sn-nw600
Co(III) Co_3O_4	779.6	779.6	779.6
Co(II) Co_3O_4	780.7	780.9, 782.2	781.5
Co(II) CoO	780.5	780.0, 782.1	
Co(II) ss CoO [a]	786.4	786.5	784.0
Co(II) ss Co_3O_4 [b]	789.5	789.5	789.0
Separation of the Co $2p_{1/2}$-$2p_{3/2}$ spin orbit components, eV			15.3

[a]Shake-up satellite of Co(II) in CoO structure. [b]Shake-up satellite of Co(II) in Co_3O_4 structure.

Fig. 1 Structure of $CoC_{22}H_{26}N_4O_2F_6$ complex.

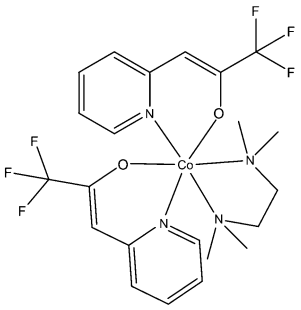

Fig. 2 HAADF-STEM image and EDX-STEM maps of Co5Sn-nw500 sample.

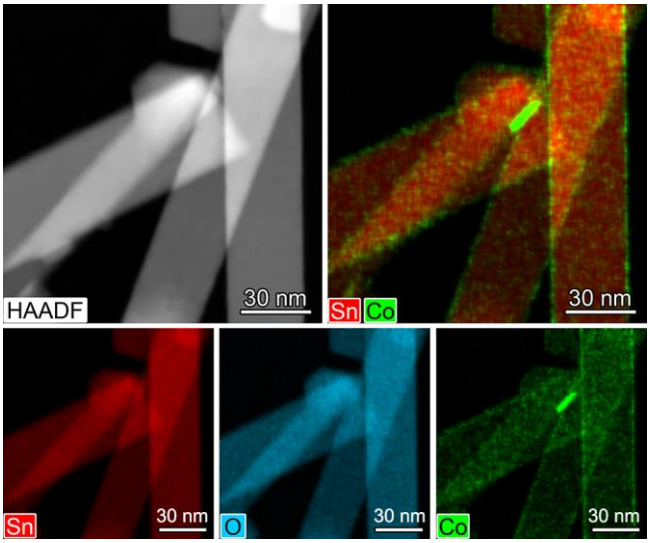

Fig. 3 HAADF-STEM image and EDX-STEM maps of Co10Sn-nw600 sample.

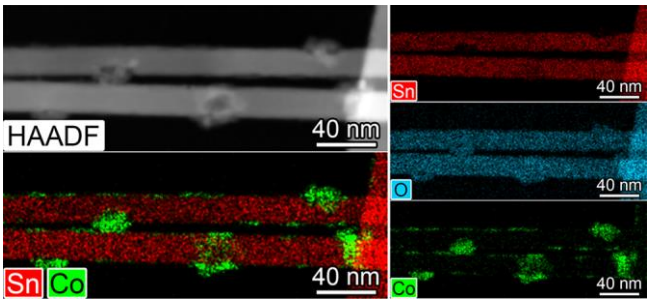

Fig. 4 X-ray diffraction patterns of CoXSn-nw nanostructures: (1) – Co5Sn-nw500, (2) – Co10Sn-nw600. Dot and dash-dot lines correspond to the reflection positions of SnO_2 and Co_3O_4, respectively.

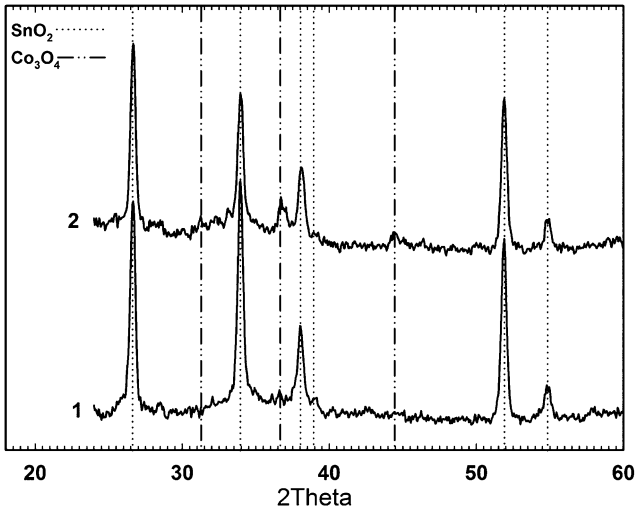

Fig. 5 Sn 3d (a), O 1s (b) and Co 2p (c) XP spectra of Co10Sn-nw600 sample. Co 2p XP-spectra are fitted by 4 doublets corresponding to Co(III) (black) and Co(II) (red) main peaks and Co(II) shake-up satellites, corresponding to Co_3O_4 (green) and CoO (pink) environment.

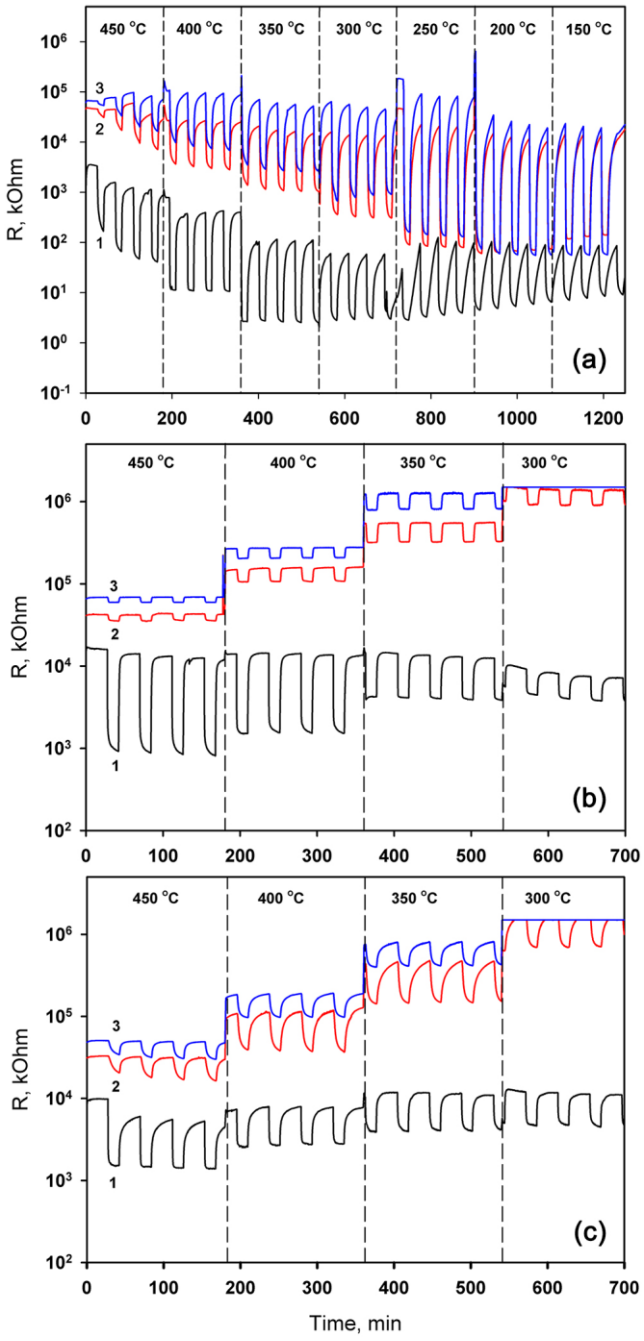

Fig. 6 Electrical response of SnO_2 nanowires and CoXSn-nw nanostructures to the periodical change of gas phase composition from dry air to gas mixtures containing 2 ppm H_2S (a), 14 ppm CO (b), or 21 ppm NH_3 (c) in dry air: (1) – SnO_2, (2) – Co5Sn-nw500, (3) – Co10Sn-nw600.

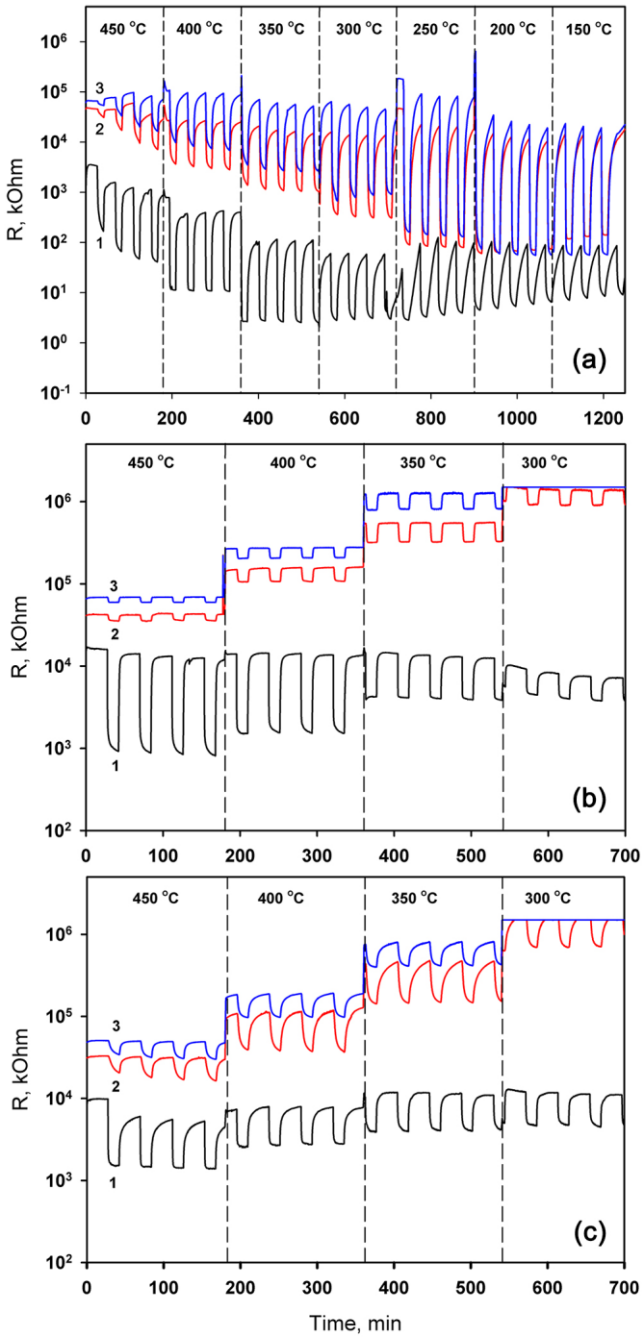

Fig. 7 Temperature dependences of sensor response *S* of SnO_2 nanowires and CoXSn-nw nanostructures to 2 ppm H_2S (a), 14 ppm CO (b), 21 ppm NH_3 (c) in dry air: (1) – SnO_2, (2) – Co5Sn-nw500, (3) – Co10Sn-nw600.

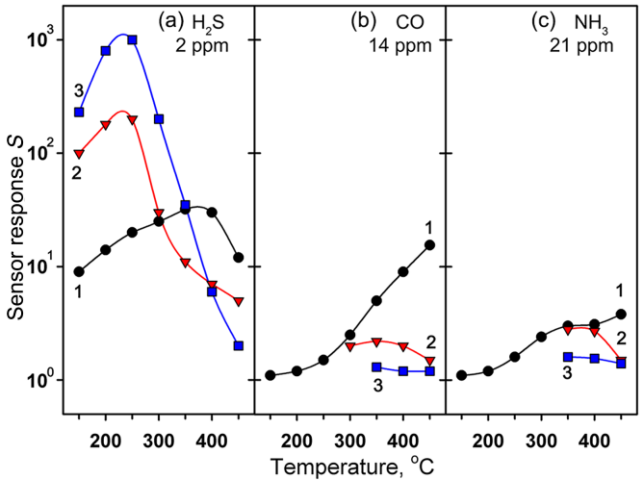

Fig. 8 Maximum sensor response to CO (14 ppm), NH_3 (21 ppm), and H_2S (2 ppm) for SnO_2 nanowires (1), Co5Sn-nw500 (2), and Co10Sn-nw600 (3).

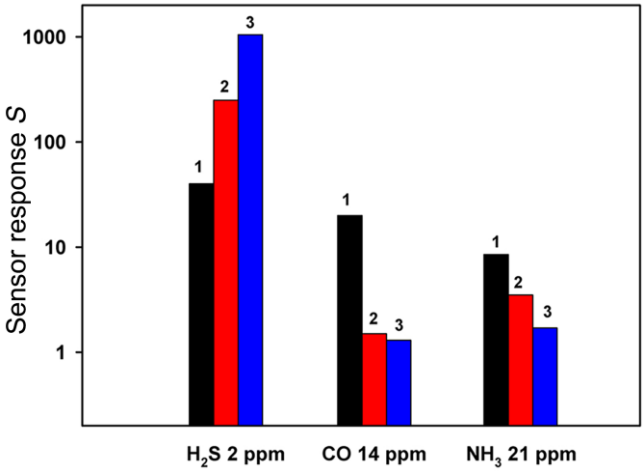

Fig. 9 X-ray diffraction patterns of Co10Sn750 nanocomposite before (1) and after interaction with H_2S (2). Arrows indicate the positions of Co_3O_4 (black) and cobalt sulfide (red) diffraction peaks. Asterisks denote SnO_2 diffraction peaks.

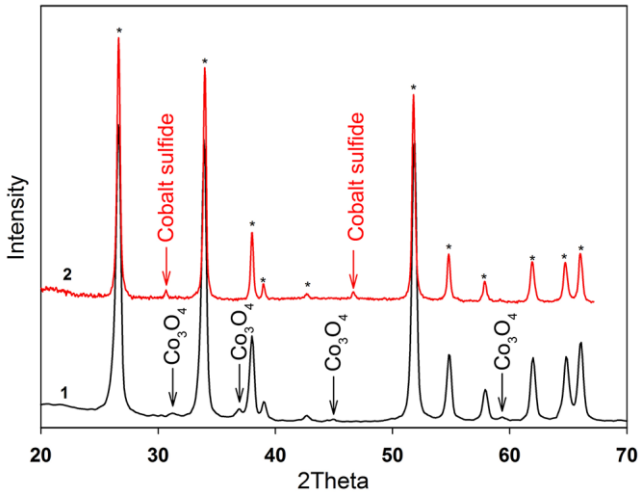

Fig. 10 Energy band diagram illustrating the formation of the *p*-Co_3O_4/*n*-SnO_2 heterojunction and its breakup in H_2S containing atmosphere.